
On the expressive power of deep neural networks

Maithra Raghu

Google Brain and Cornell University

Ben Poole

Stanford University and Google Brain

Jon Kleinberg

Cornell University

Surya Ganguli

Stanford University

Jascha Sohl-Dickstein

Google Brain

Abstract

We study the effects of the depth and width of a neural network on its *expressive power*. Precise theoretical and experimental results are derived in the generic setting of *neural networks after random initialization*. We find that three different measures of functional expressivity: number of transitions (a measure of non-linearity/complexity), network activation patterns (a new definition with an intrinsic link to hyperplane arrangements in input space) and number of dichotomies, show an exponential dependence on depth but not width. These three measures are related to each other, and, are also directly proportional to a fourth quantity, *trajectory length*. Most crucially, we show, both theoretically and experimentally, that trajectory length grows exponentially with depth, which is *why* all three measures display an exponential dependence on depth.

These results also suggest that parameters earlier in the network have greater influence over the expressive power of the network. So for any layer, its influence on expressivity is determined by the *remaining depth* of the network after that layer, which is supported by experiments on fully connected and convolutional networks on MNIST and CIFAR-10.

1 Introduction

Neural network architectures have proven “unreasonably effective” [1, 2] on many tasks, including image classification [3], identifying particles in high energy physics [4], playing Go [5], and modeling human student learning [6]. Despite their power, we have limited understanding of how and why neural networks work, and much of this understanding is qualitative and heuristic rather than precise and quantitative. While even qualitative knowledge is helpful, a more formal and fundamental framework is desperately needed to ease the laborious process of designing and training these networks, as well as to enable us to better predict and protect against their failures.

In order to develop theoretical underpinnings for deep networks, it is first necessary to disentangle the many factors that influence their effectiveness. The effectiveness of deep neural networks on real tasks can be interpreted in terms of three broad properties: their *trainability*, or how well they can be fit to data; their *generalizability*, or how well they perform on novel examples; and their *expressivity*, or the set of functions they can compute.

All three of these properties are crucial for understanding the performance of neural networks. Indeed, for success at a particular task, neural nets must first be effectively trained on a dataset, a difficult non-convex optimization problem. This has prompted investigation into properties of objective function landscape of neural networks [7, 8, 9], and the design of optimization procedures specifically suited to neural networks [10]. Trained networks must also be capable of generalizing to unseen data, and understanding generalization in neural networks is also an active line of research: [11] bounds generalization error in terms of stochastic gradient descent steps, [12, 13, 14] study generalization error through VC dimension, and [15] looks at developing smaller models with better generalization.

1.1 Expressivity

In this paper, we focus on the third of these properties, *expressivity* — the capability of neural networks to accurately represent different kinds of functions. In particular, we examine the effect of the depth and width of a neural network after *random initialization* on three different natural measures of functional richness:

- (1) Number of transitions
- (2) Activation patterns
- (3) Number of dichotomies

We intuit links between *all* the measures and another quantity, *trajectory length*, which explains the experimental observations of exponential dependence on depth for all three measures.

Activation patterns are also a natural framework to examine how a deep network subdivides input space into regions, each corresponding to a different linear function. We show that activation patterns across all layers subdivide input space into convex polytopes, and develop an asymptotically tight upper bound on the number of polytopes.

Our empirical and theoretical results connecting transitions and dichotomies to trajectory length also suggest that parameters earlier in the network should be able to ‘control’ parameters later in the network. In other words, the influence on expressivity of parameters, and thus layers, is directly related to the *remaining depth* of the network after that layer. Experiments on MNIST and CIFAR-10 support this hypothesis — training only earlier layers leads to higher accuracy than training only later layers.

1.1.1 Prior Work

The topic of neural network expressivity has a rich history, with different notions of expressivity studied. A particularly popular method of analysis has been examining *achievable functions*, the set of functions that are expressible by a fixed neural network architecture.

This approach has yielded many fascinating results: neural networks have been shown to be universal approximators [16, 17], their VC dimension studied [12, 13, 14], and connections between boolean and threshold networks and ReLU networks developed in [18, 19].

Looking at achievable functions also provides a method to compare different neural network architectures. A typical approach to this constructs classes of functions from one network architecture that another is incapable of approximating efficiently [20, 21, 22, 23]. This is often used to suggest the benefits of deep networks over shallow networks.

Other work examines the complexity of a single function computed by a deep network, rather than the complexity of a set of functions. The number of linear regions was introduced as a measure of expressivity in [24]. In [25], it was shown that a specific network achieves an exponential number of linear regions with depth. (See Section 2.3 for a generalization of linear regions to network activation patterns, and a tight upper bound on the number of achievable activation patterns saturated by the construction in [25].)

1.1.2 Paper Setting

These results, while compelling, also highlight limitations of much of the existing work on expressivity. Prior work on achievable functions contains unrealistic assumptions about the structure of the network. For instance, the universal approximation theorem also requires layers to be exponentially wide and very specific weight settings. The latter is a feature in much of the existing work on expressivity, where ‘hardcoded’ weight values or a very specific choice of function are used to illustrate the advantages of one architecture over another.

Comparing architectures in such a fashion limits the generality of the conclusions, and does not satisfactorily address the goal of understanding expressivity — to provide characteristic properties of *generic* networks for many typical tasks.

Random networks To address this, we focus on a family of networks arising in practice — the behaviour of networks after *random initialization*. There are two important advantages of this perspective:

- (1) Conclusions from examining random networks are likely to be more general than those drawn from one hardcoded weight setting, or the inapproximability of one particular function by a particular architecture.
- (2) Results on random nets also provide a natural baseline to compare and contrast trained networks with, as random initialization is the starting point to most training methods.

The expressivity of these *random networks* is largely unexplored, though a connection between random networks and compositional kernels is developed in [26].

Measures of Expressivity and Trajectory Length We provide a brief overview of the three measures of expressivity introduced in Section 1.1. They will be formally defined in Section 2.1.

- **Transitions:** Counting neuron transitions is introduced indirectly via linear regions in [24], and provides a tractable method to estimate the non-linearity of the computed function.
- **Activation Patterns:**
 - Transitions of a single neuron can be extended to the outputs of all neurons in all layers, leading to the (global) definition of a network *activation pattern*. Counting different activation patterns of a particular network is also a measure of non-linearity.
 - Far more importantly, network activation patterns directly show how the *entire* network partitions input space (into *convex polytopes*), such that the same network activation pattern cannot occur more than once along a straight line in input space. We study this, and a tight upper bound for the number of such activation patterns, in Section 2.3, through a novel connection to the theory of *hyperplane arrangements*.
- **Dichotomies:**
 - The previous two measures give an indication of the complexity of a typical random network. We also count the number of different dichotomies achieved by a *family* of random networks on a fixed input set. We show this measure is ‘statistically dual’ to sweeping inputs.
 - A striking result is that even though dichotomies are measured on *random data*, we still see an exponential increase with depth. This is a counterexample to the common belief that the power of depth stems from a correspondence between deep architectures and the structure inherent in natural data (e.g. compositionality [27], translation invariance [28], also explored in [29].)

Remaining depth All of these results suggest that the importance of a layer in a network is related to the *remaining depth* of the network after that layer. We support this observation by training single layers in isolation in a random deep network, for classification tasks on MNIST and CIFAR-10. We observe monotonically decreasing performance with decreasing remaining depth – i.e. the layers with the greatest expressive power are those which occur earliest in the network (Section 4 and Figures 7, 8, 9).

In a companion paper [30] we explore closely related questions by using dynamical mean field theory to explore the propagation of Riemannian curvature through deep networks.

2 Exponential Expressivity

The paper is structured as follows:

- 1) The theoretical result on the exponential growth of trajectory length is presented in Section 2.2, with Figure 2 providing empirical verification.
- 2) The link between trajectory length and number of transitions is intuited in Section 2.2.2 with empirical verification in many practical cases in Figure 3, and further theoretical proof in the special large weight limit case (Section 2.2.3).

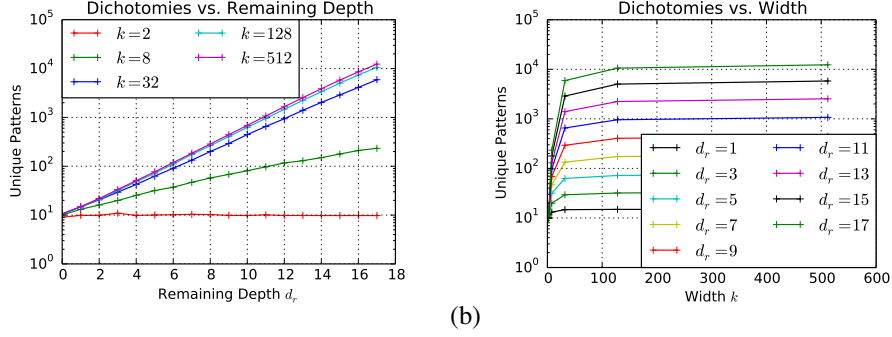


Figure 1: The number of functions achievable in a deep hard-tanh network by sweeping a single layer’s weights along a one dimensional trajectory is exponential in the remaining depth, but increases only slowly with network width. Here we plot the number of classification dichotomies over $s = 15$ input vectors achieved by sweeping the first layer weights in a hard-tanh network along a one-dimensional great circle trajectory. We show this (a) as a function of remaining depth for several widths, and (b) as a function of width for several remaining depths. All networks were generated with weight variance $\sigma_w^2 = 8$, and bias variance $\sigma_b^2 = 0$.

- 3) Section 2.3 then looks at activation patterns, discussing the relation to transitions (Corollary 2), and most importantly, relating activation patterns to hyperplane arrangements, demonstrating the partitioning of input space (Theorem 3, Figure 4) and tightly upper bounding the number of activation patterns (Theorem 5.)
- 4) Section 3 considers dichotomies, showing a statistical duality between transitions and dichotomies, verified empirically (Figure 5) which also serves to connect dichotomies and trajectory length, explaining their exponential dependence on depth (Figure 1.)
- 5) The results on dichotomies, where we sweep weights in a single layer through a trajectory, leads to the suppositions that the expressive power of a particular layer is related to the remaining depth of the network after that layer. This is supported by experiments on networks trained on MNIST and CIFAR-10 (Section 4).

2.1 Notation and Definitions

Let F_W denote a neural network. In this section, we consider architectures with input dimension m , n hidden layers all of width k , and a scalar readout layer. (So, $F_W : \mathbb{R}^m \rightarrow \mathbb{R}$.)

We use $v_i^{(d)}$ to denote the i^{th} neuron in hidden layer d . We also let $x = z^{(0)}$ be an input, $h^{(d)}$ be the hidden representation at layer d , and ϕ the non-linearity. The weights and bias are called $W^{(d)}$ and $b^{(d)}$ respectively. So we have the relations

$$h^{(d)} = W^{(d)}z^{(d)} + b^{(d)}, \quad z^{(d+1)} = \phi(h^{(d)}). \quad (1)$$

Our results mostly examine the cases where ϕ is a hard-tanh [31] or ReLU nonlinearity. All hard-tanh results carry over to tanh with additional technical steps.

We list some important definitions below:

- (1) A neuron *transitions* when it switches linear region in its activation function (i.e. for ReLU, switching between zero and linear regimes, for hard-tanh, switching between negative saturation, unsaturated and positive saturation).
- (2) For hard-tanh, we refer to a *sign transition* as the neuron switching sign, and a *saturation transition* as switching from being saturated between ± 1 .
- (3) The *Activation Pattern* of the entire network is defined by the output regions of every neuron. More precisely, given an input x , we let $\mathcal{A}(F_W, x)$ be a vector representing the activation region of every hidden neuron in the network. So for a ReLU network F_W , we can take $\mathcal{A}(F_W, x) \in \{-1, 1\}^{nk}$ with -1 meaning the neuron is in the zero regime, and 1 meaning

it is in the linear regime. For hard-tanh network F_W , we can (overloading notation slightly) take $\mathcal{A}(F_W, x) \in \{-1, 0, 1\}^{nk}$. The use of this notation will be clear by context.

(4) Given a set of inputs S , we say a *dichotomy* over S is a labeling of each point in S as ± 1 .

Random networks: We assume the weight matrices of our neural networks are initialized as random Gaussian matrices, with appropriate variance scaling to account for width, i.e. $W_{ij}^{(d)} \sim \mathcal{N}(0, \sigma_w^2/k)$. We draw biases $b_i^{(d)} \sim \mathcal{N}(0, \sigma_b^2)$.

Sweeping Input: In the analysis below, we sweep through a one dimensional input trajectory $x(t)$. The results hold for almost any such smooth $x(t)$, provided that at any point $x(t)$, the trajectory direction has some non-zero magnitude perpendicular to $x(t)$.

2.2 Neuron transitions and trajectory length

In this section, we analyze the number of sign transitions of F_W , a random hard-tanh neural network, as the input $x(t)$ is swept through a one dimensional trajectory. We rigorously derive how the length of the input curve $x(t)$ changes as it propagates through F_W . We then verify experimentally, and derive theoretically for the large weight limit, a linear relation between trajectory length and number of transitions.

2.2.1 Bound on trajectory length growth

We would like to understand how the arc length of a one dimensional trajectory $x(t)$ changes as it is pushed through a network F_W . We prove: (with a more exact lower bound in the Appendix)

Theorem 1. Bound on Growth of Trajectory Length *Let F_W be a hard tanh random neural network and $x(t)$ a one dimensional trajectory in input space. Define $z^{(d)}(x(t)) = z^{(d)}(t)$ to be the image of the trajectory in layer d of F_W , and let $l(z^{(d)}(t)) = \int_t \left\| \frac{dz^{(d)}(t)}{dt} \right\| dt$ be the arc length of $z^{(d)}(t)$. Then*

$$\mathbb{E} \left[l(z^{(d)}(t)) \right] \geq O \left(\left(\frac{\sigma_w}{(\sigma_w^2 + \sigma_b^2)^{1/4}} \cdot \frac{\sqrt{k}}{\sqrt{\sigma_w^2 + \sigma_b^2 + k}} \right)^d l(x(t)) \right)$$

This bound is *tight* in the limits of large σ_w and k . An immediate Corollary for $\sigma_b = 0$, i.e. no bias, is

Corollary 1. Bound on Growth of Trajectory Length Without Bias *For F_W with zero bias, we have*

$$\mathbb{E} \left[l(z^{(d)}(t)) \right] \geq O \left(\left(\frac{\sqrt{\sigma_w k}}{\sqrt{\sigma_w + k}} \right)^d l(x(t)) \right)$$

The theorem shows that the image of a trajectory in layer d has grown *exponentially in d* , with the scaling σ_w and width of the network k determining the base. We additionally state and prove a simple $O(\sigma_w^d)$ growth upper bound in the Appendix. Figure 2 demonstrates this behavior in simulation, and compares against the bounds. Note also that if the variance of the bias is comparatively too large i.e. $\sigma_b \gg \sigma_w$, then we no longer see exponential growth. This phase transition behavior is explored further in our companion paper [30].

The proof can be found in the Appendix. A rough outline is as follows: to prove this growth rate, instead of working with the integral form, we look at the expected growth of the difference between a point $z^{(d)}(t)$ on the curve and a small perturbation $z^{(d)}(t + dt)$, from layer d to layer $d + 1$. Denoting this quantity $\|\delta z^{(d)}(t)\|$, we derive a recurrence relating $\|\delta z^{(d+1)}(t)\|$ and $\|\delta z^{(d)}(t)\|$ which can be composed to give the desired growth rate.

The analysis contains an additional layer of complexity, as for tractability we need statistical independence from the image of the input $z^{(d+1)}(t)$. So we instead form a recursion by looking at the component of the difference perpendicular to the image of the input in that layer, i.e. $\|\delta z_{\perp}^{(d+1)}(t)\|$.

For a typical trajectory, the perpendicular component preserves a fraction $\sqrt{\frac{k-1}{k}}$ of the total trajectory

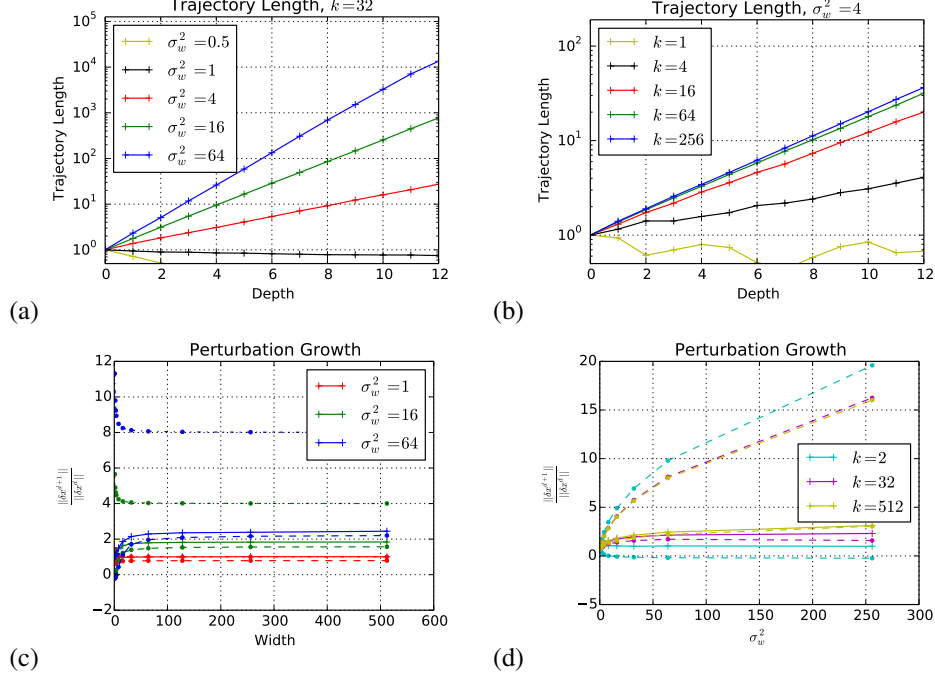


Figure 2: The exponential growth of trajectory length with depth, in a random deep network with hard-tanh nonlinearities. A trajectory is chosen in input space performing a great circle interpolation between two random vectors. The image of that trajectory is taken at each layer of the network, and its length measured. (a,b) The trajectory length vs. layer, in terms of the network width k and weight variance σ_w^2 , both of which determine its growth rate. (c,d) The average ratio of a trajectory’s length in layer $d+1$ relative to its length in layer d . The solid line shows simulated data, while the dashed lines show upper and lower bounds (Theorem 1). Growth rate is a function of layer width k , and weight variance σ_w^2 .

length, and our derived growth rate thus provides a close lower bound, as demonstrated in Figure 2(c,d).

We further discuss the properties of this growth rate in several regimes of interest in Section 2.2.3.

2.2.2 Relation to number of transitions

To understand the relation to the number of sign transitions, observe the following: for F_W with n hidden layers as above, the linear, one dimensional, readout layer outputs a value by computing the inner product $W^{(n)} z^{(n)}$. The sign of the output is then determined by whether this quantity is ≥ 0 or not. In particular, the decision boundary is a *hyperplane*, with equation $W^{(n)} z^{(n)} = 0$.

The number of transitions we see the output neuron make as $x(t)$ is traced in the input is then exactly the number of times $z^{(n)}(t)$ crosses the decision boundary. As F_W is a random neural network, with signs of weight entries split purely randomly between ± 1 , we expect to see a direct proportionality between the length of the curve $z^{(n)}(t)$, and the number of times it crosses the decision boundary. This is unequivocally demonstrated by our experimental results in Figure 3. In Theorem 2 we prove this relationship for the large σ_w limit. We state it as an observation below:

Observation 1. In a random neural network F_W with hard-tanh activations, the expected number of sign transitions induced by a one dimensional curve $x(t)$ in the input is directly proportional to the length of the latent image of the curve, $z^{(n)}(t)$.

In Section 3 we discuss the implications of this result for the number of unique dichotomies on inputs we see arising from a class of functions $\{F_W\}$.

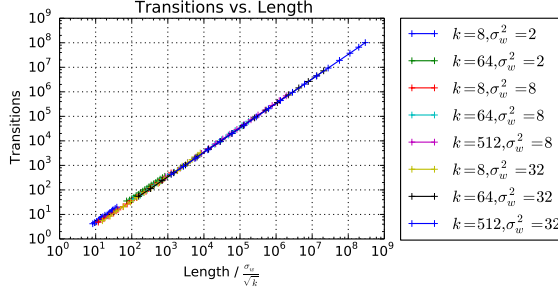


Figure 3: The number of transitions is linear in trajectory length. Here we compare the empirical number of sign changes to the length of the trajectory, for images of the same trajectory at different layers of a hard-tanh network. We repeat this comparison for a variety of network architectures, with different network width k and weight variance σ_w^2 .

2.2.3 Trajectory length growth in different regimes

Returning to the statement of Theorem 1, we can consider what the trajectory length growth (and therefore number of transitions) looks like for different choices of k and σ_w . We see that for very large k , the trajectory length is exponential in the depth with base only dependent on σ_w . This appears intuitively correct, as for very large k , we expect to see a normalizing effect caused by the Central Limit Theorem – we sum together a very large number of independent random variables (for each neuron), and perform an implicit averaging through setting the variance of each weight coordinate to be σ_w^2/k .

For very large σ_w , we see that the base of exponential growth is now \sqrt{k} . This ‘large weight limit’ results in very tractable behavior, because:

- (1) For any input (bounded away from zero) almost all neurons are saturated
- (2) Any neuron transitioning from 1 to -1 or vice versa over an interval $x(t), x(t + \Delta t)$ does so almost instantaneously. As a consequence, can assume that at most one neuron within a layer is transitioning at any point.

Under these two assumptions, we prove:

Theorem 2. Number of transitions in large weight limit *Given F_W , a random neural network with hard-tanh activations, in the very large σ_w regime, the number of sign transitions of the network as an input $x(t)$ is swept is:*

(i) For $\sigma_b = 0$: $O((\sqrt{k})^n)$

(ii) For $\sigma_b > 0$:

$$O\left(\left(\frac{\sqrt{k}}{\sqrt{1 + \frac{\sigma_b^2}{\sigma_w^2}}}\right)^n\right)$$

which is a specific case of Observation 1. The full proof is in the Appendix, and reduces the problem to one of the relative magnitudes of independent Gaussians.

2.3 A Global Perspective: Transitions and Activation Patterns

Previously, we related input trajectory growth to a ‘local’ notion of expressivity, sign transitions of a single neuron. In fact, this local measure of expressivity has an elegant connection to the ‘global’ notion of expressivity of the number of *activation patterns* of a network. We can show, that for many well-behaved trajectories, the number of transitions (which is directly proportional to trajectory length) is exactly equal to the number of unique activation patterns.

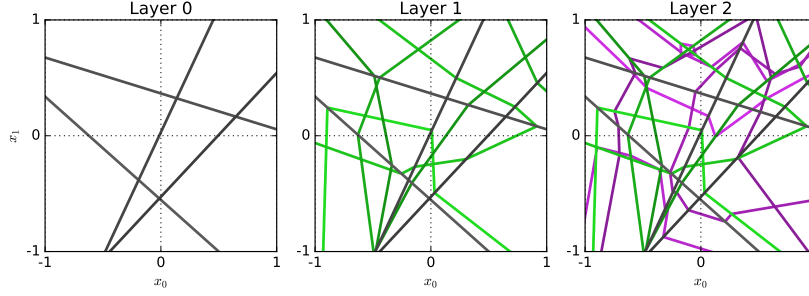


Figure 4: Deep networks with piecewise linear activations subdivide input space into convex polytopes. Here we plot the boundaries in input space separating unit activation and inactivation for all units in a three layer ReLU network, with four units in each layer. The left pane shows activation boundaries in gray for the first layer only. These correspond to hyperplanes. The center pane shows activation boundaries for the first two layers. Second layer activation boundaries in green are piecewise linear, but can bend at first layer activation boundaries. The right pane shows activation boundaries for the first three layers. The third layer activation boundaries in purple are also piecewise linear, but can bend when the active set changes in either of the first two layers. Each convex polytope formed by these activation boundaries corresponds to a unique pattern of activation across the entire network.

A helpful mental picture is obtained through the language of *hyperplane arrangements*. A hyperplane arrangement consists of a set of hyperplanes in an ambient space, in our case the input space \mathbb{R}^m . An arrangement of this fashion divides up \mathbb{R}^m into *regions*.

Hyperplanes relate to neural networks in the following way: consider a ReLU random neural network. Given a particular neuron in the first layer, we can ask for which inputs it is ‘on’ (the linear regime), and for which inputs it is ‘off’ (the zero regime). This ‘boundary’ in the input space is a hyperplane defined by the points x for which the inner product of x with the weights into the neuron (plus a bias term) are zero. Drawing a hyperplane for every neuron in the first layer then gives a hyperplane arrangement, with every region of this arrangement in *one-to-one* correspondence with a particular subset of neurons being active.

The next crucial insight is realizing we can apply a similar analysis to the second layer: in particular, inside a particular region of the hyperplane arrangement defined by the first layer, a *linear* function of the input passes into the second layer. This means we can consider the on/off patterns of the second layer within this region, which defines another hyperplane arrangement *subdividing* this particular region into sub-regions. Applying this over all regions gives convex sub-divisions of the input space which are in one to one correspondence with the neuron activation patterns in the first and second layers.

Figure 4 illustrates this subdivision of input space into convex polytopes. We make this precise in the theorem below, establishing a bijection between activation patterns of F_W (for hard tanh and ReLU activations) and regions in input space.

Theorem 3. *Regions in Input Space Suppose $F_W : \mathbb{R}^m \rightarrow \mathbb{R}$, with ReLU or hard-tanh activations. The set of activation patterns of F_W (activation patterns across all layers in the network) partitions the input space into convex regions (by definition bounded and unbounded polytopes), one for each activation pattern.*

Proof. We show inductively that F_W partitions the input space into convex polytopes via hyperplanes. Consider the image of the input space under the first hidden layer. Each neuron $v_i^{(1)}$ defines hyperplane(s) on the input space: letting $W_i^{(0)}$ be the i th row of $W^{(0)}$, $b_i^{(0)}$ the bias, we have the hyperplane $W_i^{(0)}x + b_i = 0$ for a ReLU and hyperplanes $W_i^{(0)}x + b_i = \pm 1$ for a hard-tanh. Considering all such hyperplanes over neurons in the first layer, we get a hyperplane arrangement in the input space, each polytope corresponding to a specific activation pattern in the first hidden layer.

Now, assume we have partitioned our input space into convex polytopes with hyperplanes from layers $\leq d - 1$. Consider $v_i^{(d)}$ and a specific polytope R_i . Then the activation pattern on layers $\leq d - 1$

is constant on R_i , and so the input to $v_i^{(d)}$ on R_i is a linear function of the inputs $\sum_j \lambda_j x_j + b$ and some constant term, comprising of the bias and the output of saturated units. Setting this expression to zero (for ReLUs) or to ± 1 (for hard-tanh) again gives a hyperplane equation, but this time, the equation is only valid in R_i (as we get a different linear function of the inputs in a different region.) So the defined hyperplane(s) either partition R_i (if they intersect R_i) or the output pattern of $v_i^{(d)}$ is also constant on R_i . The theorem then follows. \square

This implies that any one dimensional trajectory $x(t)$, that does not ‘double back’ on itself (i.e. reenter a polytope it has previously passed through), will not repeat activation patterns. In particular, after seeing a transition (crossing a hyperplane to a different region in input space) we will never return to the region we left. A simple example of such a trajectory is a straight line:

Corollary 2. Transitions and Output Patterns in an Affine Trajectory *For any affine one dimensional trajectory $x(t) = x_0 + t(x_1 - x_0)$ input into a neural network F_W , we partition $\mathbb{R} \ni t$ into intervals every time a neuron transitions. No two partitions have the same neuron output pattern on F_W .*

With the picture of the input space split into regions, the next natural question is to ask how many regions we can achieve. In other words, how many neuron output patterns (activation/saturation) can we see over the entire input? Considering a region R in the input space as in the proof of Theorem 3, we see that we have at most k (for ReLUs) or $2k$ (for hard-tanh) hyperplanes, in $R \subset \mathbb{R}^m$. So a first step is determining how many regions we get when we have k hyperplanes in \mathbb{R}^m . The question of the number of regions for a specific hyperplane arrangement is well studied [32], with many beautiful abstract constructions, such as *intersection posets*. Here we prove an upper bound on the number of regions induced by a hyperplane arrangement:

Theorem 4. Upper Bound on Regions in a Hyperplane Arrangement *Suppose we have k hyperplanes in \mathbb{R}^m - i.e. k equations of form $\alpha_i x = \beta_i$. for $\alpha_i \in \mathbb{R}^m$, $\beta_i \in \mathbb{R}$. Let the number of regions (connected open sets bounded on some sides by the hyperplanes) be $r(k, m)$. Then*

$$r(k, m) \leq \sum_{i=0}^m \binom{k}{i}$$

The full proof is in the Appendix, and relies on the elegant recursion $r(k, m) = r(k-1, m-1) + r(k-1, m)$ combined with an induction.

With this result, we conclude that when considering the effect of layer d on the existing regions, each existing region can be partitioned into at most $r(k, m)$ subregions (or for hard-tanh, $r(2k, m)$.) So an upper bound on the number of regions (and therefore, activation patterns) achievable through this is given by $(r(k, m))^n$, i.e. we have proved:

Theorem 5. (Tight) Upper bound for Number of Activation Patterns *Given a neural network F_W , inputs in \mathbb{R}^m , with ReLU or hard-tanh activations, and with n hidden layers of width k , the number of activation patterns grows at most like $O(k^{mn})$ for ReLU, or $O((2k)^{mn})$ for hard-tanh.*

In [25], it is observed that a (trivial) upper bound is given by 2^{kmn} (all possible subsets of all possible neurons), and a construction is given for which the number of linear regions increases exponentially with depth. The upper bound we give in Theorem 5 is exponentially smaller, and is shown to be asymptotically tight by the construction in [25].

3 Function Space

3.1 The Dual Perspective

In the previous sections, we have examined the effect of depth and width on the expressivity of a neural network when varying an input x along a one dimensional trajectory in input space. The supporting experiments show that even for simple trajectories, e.g. interpolating a line or circular arc, we observe the characteristic properties of exponential increase of curve length, transitions, and output patterns with depth.

A dual perspective to sweeping the inputs over a trajectory $x(t)$ while holding the weights $W^{(0)}$ fixed, is to instead view the trajectory as sweeping the first layer *weights* along some trajectory

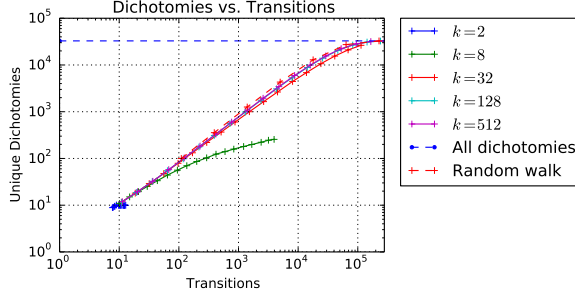


Figure 5: As the network width k increases, moving along a trajectory in the first layer weights increasingly resembles a random walk over dichotomies. Here we plot the number of unique dichotomies that have been observed as a function of the number of transitions the network has undergone. Each datapoint corresponds to the number of transitions and dichotomies for a hard-tanh network of a different depth, with the weights in the first layer undergoing interpolation along a great circle trajectory $W^{(0)}(t)$. We compare these plots to a random walk simulation, where at each transition a single class label is flipped uniformly at random. Dichotomies are measured over a dataset consisting of $s = 15$ random samples, and all networks had weight variance $\sigma_w^2 = 16$. The blue dashed line indicates all 2^s possible dichotomies.

$W^{(0)}(t)$ while holding the inputs x fixed. More formally, if we pick two random inputs, x, x' , and consider the arc $x \cos(t) + x' \sin(t)$, our first layer input is $Wx \cos(t) + Wx' \sin(t)$. Instead, we could view a rotation as picking two random *matrices*, W, W' , and doing a circular interpolation $W \cos(t) + W' \sin(t)$ over weight matrices. Our different inputs are then Wx and $W'x$. This is not an exact duality – there is a rotation in weight space corresponding to any rotation in input space, but there is not a rotation in input space corresponding to any rotation in weight space. However, it provides a natural dual analogue for random inputs, changing an analysis over sweeping inputs, to a *function class* \mathcal{F} produced by sweeping over weights.

Having shifted perspective to consider function classes, a natural question is understanding how *heterogeneous* this they are. One way to measure this is to consider the set of dichotomies this function class gives over a set of (random) inputs. More precisely, given a set of inputs, $S = \{x_1, \dots, x_s\} \subset \mathbb{R}^m$, how many of the 2^s possible dichotomies does this function class produce on S ?

For non-random inputs and non-random functions, this is a well known question closely related to the VC dimension of the function class, and upper bounded by the Sauer-Shelah lemma [33]. We discuss this further in Appendix D.1.

Previously we’ve seen, theoretically and experimentally, that growth in trajectory length (influenced by depth and width) is linearly related to the number of transitions. Also, if the $x_i \in S$ are sufficiently uncorrelated (e.g. random) class label transitions should occur independently for each x_i . Together, this would suggest:

Observation 2. Depth and Expressivity in a Function Class. Given the function class \mathcal{F} as above, the number of dichotomies expressible by \mathcal{F} over a set of random inputs S by sweeping the first layer weights along a one dimensional trajectory $W^{(0)}(t)$ is exponential in the network depth n .

This is unambiguously supported by the growth in the number of dichotomies with depth in Figure 1. This is further supported by an exponential decrease in autocorrelation length in function space, which we derive in the Supplemental Material of our companion paper [30].

Our results further suggest the following conjectures:

Conjecture 1. As network width k increases, the exploration of the space of dichotomies increasingly resembles a simple random walk on a hypercube with dimension equal to the number of inputs $|S|$.

This conjecture is supported by Figure 5, which compares the number of unique dichotomies achieved by networks of various widths to the number of unique dichotomies achieved by a random walk.

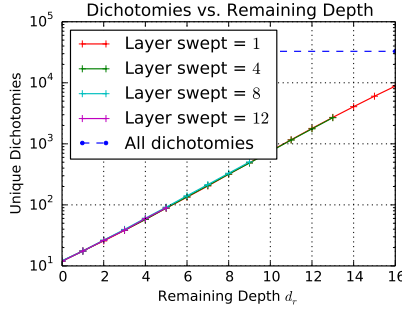


Figure 6: Expressive power depends only on remaining network depth. Here we plot the number of dichotomies achieved by sweeping the weights in different network layers through a 1-dimensional great circle trajectory, as a function of the remaining network depth. The number of achievable dichotomies does not depend on the total network depth, only on the number of layers above the layer swept. All networks had width $k = 128$, weight variance $\sigma_w^2 = 8$, number of datapoints $s = 15$, and hard-tanh nonlinearities. The blue dashed line indicates all 2^s possible dichotomies for this random dataset.

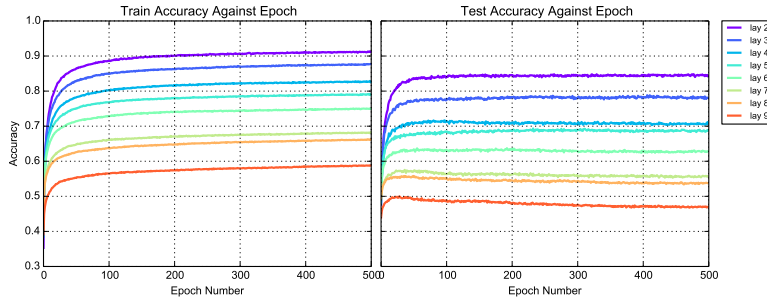


Figure 7: Demonstration of expressive power of remaining depth on MNIST. Here we plot train and test accuracy achieved by training exactly one layer of a fully connected neural net on MNIST. The different lines are generated by varying the hidden layer chosen to train. All other layers are kept frozen after random initialization. We see that training lower hidden layers leads to better performance. The networks had width $k = 100$, weight variance $\sigma_w^2 = 2$, and hard-tanh nonlinearities. Note that we only train from the second hidden layer (weights $W^{(1)}$) onwards, so that the number of parameters trained remains fixed. While the theory addresses training accuracy and not generalization accuracy, the same monotonic pattern is seen for both.

Conjecture 2. *The expressive power of a single weight $W_{ij}^{(d)}$ at layer d in a random network F , and for a set of random inputs S , is exponential in the remaining network depth $d_r = (n - d)$. Here expressive power is the number of dichotomies achievable by adjusting only that weight.*

That is, the expressive power of weights in early layers in a deep hard-tanh network is exponentially greater than the expressive power of weights in later layers. This is supported by the invariance to layer number in the recurrence relations used in all proofs directly involving depth. It is also directly supported by simulation, as illustrated in Figure 6, and by experiments on MNIST and CIFAR10 as illustrated in Figures 7, 8, and 9.

4 Experiments

We implemented the random network architecture described in Section 2.1. In separate experiments we then swept an input vector along a great circle trajectory (a rotation) for fixed weights, and swept weights along a great circle trajectory for a fixed set of inputs, as described in Section 3.1. In both cases, the trajectory was subdivided into 10^6 segments. We repeated this for a grid of network widths k , weight variances σ_w^2 , and number of inputs s . Unless otherwise noted, $\sigma_b = 0$ for all experiments.

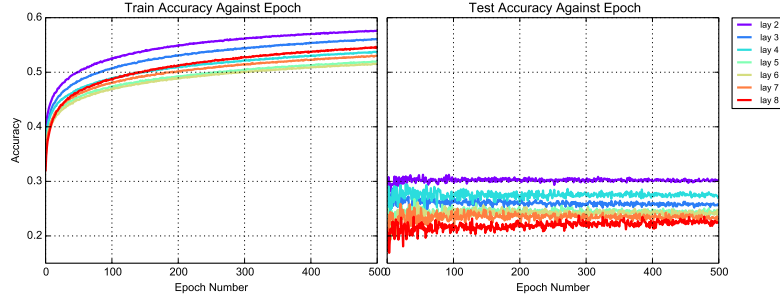


Figure 8: We repeat the experiment in Figure 7 with a fully connected network on CIFAR-10, and mostly observe that training lower layers again leads to better performance. The networks had width $k = 200$, weight variance $\sigma_w^2 = 1$, and hard-tanh nonlinearities. We again only train from the second hidden layer on so that the number of parameters remains fixed.

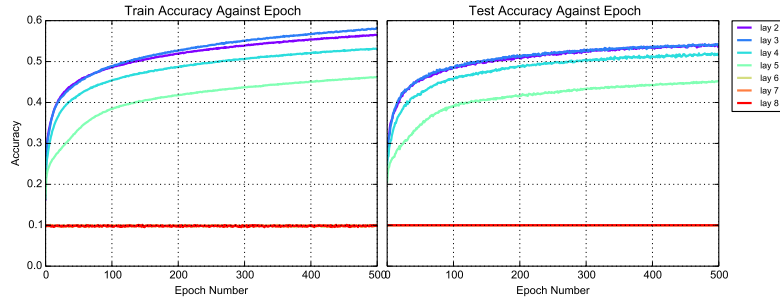


Figure 9: We repeat the experiment in Figure 7 for a convolutional network trained on CIFAR-10. The network has eight convolutional hidden layers, with three by three filters and 64 filters in each layer, all with ReLU activations. The final layer is a fully connected softmax, and is trained in addition to the single convolutional layer being trained. The results again support greater expressive power with remaining depth. Note the final three convolutional layers failed to effectively train, and performed at chance level.

We repeated each experiment 10 times and averaged over the results. The simulation results are discussed and plotted throughout the text.

We also studied the implications of these results for trained networks. In the experiments related to Figures 7, 8, 9 we randomly initialized a neural network, and froze all the layers except for one, which we trained (on MNIST and CIFAR-10). The results show that better performance results from training lower layers than from training higher layers, which supports the results on the expressive importance

Property	Architecture	Results
Trajectory length	hard-tanh	Asymptotically tight lower bound (Thm 1) Upper bound (Appendix Section A) Simulation (Fig 2)
Neuron transitions	hard-tanh	Expectation in large weight limit (Thm 2) Simulation (Fig 3)
Dichotomies	hard-tanh	Simulation (Figs 1 and 5)
Regions in input space	hard-tanh and ReLU	Consist of convex polytopes (Thm 4)
Network activation patterns	hard-tanh and ReLU	Tight upper bound (Thm 4)
Effect of remaining depth	hard-tanh	Simulation (Fig 6)
Trainable expressive power	hard-tanh	Experiment on MNIST (Fig 7) Experiments on CIFAR-10 (Figs 8 and 9)

Table 1: List and location of key theoretical and experimental results.

of remaining depth (Figure 6.) The networks were implemented using Keras and TensorFlow, and trained for a fixed number of epochs using the ADAM optimizer. To ensure fair comparisons could be made across layers, no Dropout or other regularization techniques were used. In our companion paper [30], we explore the effect of width and total depth when training only the final layer in the network.

5 Conclusion

In this paper, we studied the expressivity of neural networks with random weights. This framework enabled an *average case analysis*, and illustrated the relation between trajectory length, neuron transitions, activation patterns, and achievable classification dichotomies (see Table 1). Our analysis also provided precise theoretical and experimental results on the impact of depth and width on neural networks. In particular, greater depth results in an exponential increase of these values.

That exponentially large changes in output can be induced by small changes in the input may help explain the prevalence of *adversarial examples* [34] in deep networks. Additionally, understanding this structure may inspire new optimization schemes that account for the differing leverage of weights at different layers. The greater leverage stemming from training earlier weights may also motivate novel ways to adapt pre-trained networks to new tasks, beyond simply retraining the top layer (least expressive) weights.

We believe further ‘average case’ study of neural networks will continue to improve our understanding, and inspire practical algorithms and architectures.

Acknowledgements

We thank Samy Bengio, Ian Goodfellow, Laurent Dinh, and Quoc Le for extremely helpful discussion.

References

- [1] Yann LeCun. The unreasonable effectiveness of deep learning. In *Seminar*. Johns Hopkins University, 2014.
- [2] Andrej Karpathy. The unreasonable effectiveness of recurrent neural networks. In *Andrej Karpathy blog*, 2015.
- [3] Alex Krizhevsky, Ilya Sutskever, and Geoffrey E Hinton. Imagenet classification with deep convolutional neural networks. In *Advances in neural information processing systems*, pages 1097–1105, 2012.
- [4] Pierre Baldi, Peter Sadowski, and Daniel Whiteson. Searching for exotic particles in high-energy physics with deep learning. *Nature communications*, 5, 2014.
- [5] David Silver, Aja Huang, Chris J Maddison, Arthur Guez, Laurent Sifre, George Van Den Driessche, Julian Schrittwieser, Ioannis Antonoglou, Veda Panneershelvam, Marc Lanctot, et al. Mastering the game of go with deep neural networks and tree search. *Nature*, 529(7587):484–489, 2016.
- [6] Chris Piech, Jonathan Bassen, Jonathan Huang, Surya Ganguli, Mehran Sahami, Leonidas J Guibas, and Jascha Sohl-Dickstein. Deep knowledge tracing. In *Advances in Neural Information Processing Systems*, pages 505–513, 2015.
- [7] Yann N Dauphin, Razvan Pascanu, Caglar Gulcehre, Kyunghyun Cho, Surya Ganguli, and Yoshua Bengio. Identifying and attacking the saddle point problem in high-dimensional non-convex optimization. In *Advances in neural information processing systems*, pages 2933–2941, 2014.
- [8] Ian J Goodfellow, Oriol Vinyals, and Andrew M Saxe. Qualitatively characterizing neural network optimization problems. *arXiv preprint arXiv:1412.6544*, 2014.
- [9] Anna Choromanska, Mikael Henaff, Michael Mathieu, Gérard Ben Arous, and Yann LeCun. The loss surfaces of multilayer networks. *arXiv preprint arXiv:1412.0233*, 2014.
- [10] James Martens and Roger Grosse. Optimizing neural networks with kronecker-factored approximate curvature. *arXiv preprint arXiv:1503.05671*, 2015.
- [11] Moritz Hardt, Benjamin Recht, and Yoram Singer. Train faster, generalize better: Stability of stochastic gradient descent. *arXiv preprint arXiv:1509.01240*, 2015.
- [12] Eduardo D Sontag. Vc dimension of neural networks. *NATO ASI SERIES F COMPUTER AND SYSTEMS SCIENCES*, 168:69–96, 1998.
- [13] Peter L Bartlett and Wolfgang Maass. Vapnik-chervonenkis dimension of neural nets. *The handbook of brain theory and neural networks*, pages 1188–1192, 2003.
- [14] Peter L Bartlett, Vitaly Maiorov, and Ron Meir. Almost linear vc-dimension bounds for piecewise polynomial networks. *Neural computation*, 10(8):2159–2173, 1998.

- [15] Geoffrey Hinton, Oriol Vinyals, and Jeff Dean. Distilling the knowledge in a neural network. *arXiv preprint arXiv:1503.02531*, 2015.
- [16] Kurt Hornik, Maxwell Stinchcombe, and Halbert White. Multilayer feedforward networks are universal approximators. *Neural networks*, 2(5):359–366, 1989.
- [17] George Cybenko. Approximation by superpositions of a sigmoidal function. *Mathematics of control, signals and systems*, 2(4):303–314, 1989.
- [18] Wolfgang Maass, Georg Schnitger, and Eduardo D Sontag. *A comparison of the computational power of sigmoid and Boolean threshold circuits*. Springer, 1994.
- [19] Xingyuan Pan and Vivek Srikumar. Expressiveness of rectifier networks. *arXiv preprint arXiv:1511.05678*, 2015.
- [20] Ronen Eldan and Ohad Shamir. The power of depth for feedforward neural networks. *arXiv preprint arXiv:1512.03965*, 2015.
- [21] Matus Telgarsky. Representation benefits of deep feedforward networks. *arXiv preprint arXiv:1509.08101*, 2015.
- [22] James Martens, Arkadev Chattopadhyaya, Toni Pitassi, and Richard Zemel. On the representational efficiency of restricted boltzmann machines. In *Advances in Neural Information Processing Systems*, pages 2877–2885, 2013.
- [23] Monica Bianchini and Franco Scarselli. On the complexity of neural network classifiers: A comparison between shallow and deep architectures. *Neural Networks and Learning Systems, IEEE Transactions on*, 25(8):1553–1565, 2014.
- [24] Razvan Pascanu, Guido Montufar, and Yoshua Bengio. On the number of response regions of deep feed forward networks with piece-wise linear activations. *arXiv preprint arXiv:1312.6098*, 2013.
- [25] Guido F Montufar, Razvan Pascanu, Kyunghyun Cho, and Yoshua Bengio. On the number of linear regions of deep neural networks. In *Advances in neural information processing systems*, pages 2924–2932, 2014.
- [26] Amit Daniely, Roy Frostig, and Yoram Singer. Toward deeper understanding of neural networks: The power of initialization and a dual view on expressivity. *arXiv preprint arXiv:1602.05897*, 2016.
- [27] Hrushikesh Mhaskar, Qianli Liao, and Tomaso Poggio. Learning real and boolean functions: When is deep better than shallow. *arXiv preprint arXiv:1603.00988*, 2016.
- [28] Yann LeCun, Léon Bottou, Yoshua Bengio, and Patrick Haffner. Gradient-based learning applied to document recognition. *Proceedings of the IEEE*, 86(11):2278–2324, 1998.
- [29] Nadav Cohen, Or Sharir, and Amnon Shashua. On the expressive power of deep learning: a tensor analysis. *arXiv preprint arXiv:1509.05009*, 2015.
- [30] Ben Poole, Subhaneil Lahiri, Maithra Raghu, Jascha Sohl-Dickstein, and Surya Ganguli. Exponential expressivity in deep neural networks through transient chaos. *arXiv preprint*, 2016.
- [31] Ronan Collobert and Samy Bengio. Links between perceptrons, mlps and svms. In *Proceedings of the twenty-first international conference on Machine learning*, page 23. ACM, 2004.
- [32] Richard Stanley. Hyperplane arrangements. *Enumerative Combinatorics*, 2011.
- [33] Norbert Sauer. On the density of families of sets. *Journal of Combinatorial Theory, Series A*, 13(1): 145–147, 1972.
- [34] Christian Szegedy, Wojciech Zaremba, Ilya Sutskever, Joan Bruna, Dumitru Erhan, Ian Goodfellow, and Rob Fergus. Intriguing properties of neural networks. *arXiv preprint arXiv:1312.6199*, 2013.
- [35] D. Kershaw. Some extensions of w. gautschi’s inequalities for the gamma function. *Mathematics of Computation*, 41(164):607–611, 1983.
- [36] Andrea Laforgia and Pierpaolo Natalini. On some inequalities for the gamma function. *Advances in Dynamical Systems and Applications*, 8(2):261–267, 2013.
- [37] Vladimir Naumovich Vapnik and Vlamimir Vapnik. *Statistical learning theory*, volume 1. Wiley New York, 1998.

Appendix

Here we include the full proofs from sections in the paper.

A Proofs and additional results from Section 2.2

Proof of Theorem 1 We prove this result for F_W with zero bias for technical simplicity. The result also translates over to F_W with bias with a couple of technical modifications.

A.1 Notation and Preliminary Results

Difference of points on trajectory Given $x(t) = x, x(t + dt) = x + \delta x$ in the trajectory, let $\delta z^{(d)} = z^{(d)}(x + \delta x) - z^{(d)}(x)$

Parallel and Perpendicular Components: Given vectors x, y , we can write $y = y_\perp + y_\parallel$ where y_\perp is the component of y perpendicular to x , and y_\parallel is the component parallel to x . (Strictly speaking, these components should also have a subscript x , but we suppress it as the direction with respect to which parallel and perpendicular components are being taken will be explicitly stated.)

This notation can also be used with a matrix W , see Lemma 1.

Before stating and proving the main theorem, we need a few preliminary results.

Lemma 1. Matrix Decomposition *Let $x, y \in \mathbb{R}^k$ be fixed non-zero vectors, and let W be a (full rank) matrix. Then, we can write*

$$W = {}^\parallel W_\parallel + {}^\parallel W_\perp + {}^\perp W_\parallel + {}^\perp W_\perp$$

such that

$$\begin{aligned} {}^\parallel W_\perp x &= 0 & {}^\perp W_\perp x &= 0 \\ y^T {}^\perp W_\parallel &= 0 & y^T {}^\perp W_\perp &= 0 \end{aligned}$$

i.e. the row space of W is decomposed to perpendicular and parallel components with respect to x (subscript on right), and the column space is decomposed to perpendicular and parallel components of y (superscript on left).

Proof. Let V, U be rotations such that $Vx = (||x||, 0, \dots, 0)^T$ and $Uy = (||y||, 0, \dots, 0)^T$. Now let $\tilde{W} = UWV^T$, and let $\tilde{W} = {}^\parallel \tilde{W}_\parallel + {}^\parallel \tilde{W}_\perp + {}^\perp \tilde{W}_\parallel + {}^\perp \tilde{W}_\perp$, with ${}^\parallel \tilde{W}_\parallel$ having non-zero term exactly \tilde{W}_{11} , ${}^\parallel \tilde{W}_\perp$ having non-zero entries exactly \tilde{W}_{1i} for $2 \leq i \leq k$. Finally, we let ${}^\perp \tilde{W}_\parallel$ have non-zero entries exactly \tilde{W}_{i1} , with $2 \leq i \leq k$ and ${}^\perp \tilde{W}_\perp$ have the remaining entries non-zero.

If we define $\tilde{x} = Vx$ and $\tilde{y} = Uy$, then we see that

$$\begin{aligned} {}^\parallel \tilde{W}_\perp \tilde{x} &= 0 & {}^\perp \tilde{W}_\perp \tilde{x} &= 0 \\ \tilde{y}^T {}^\perp \tilde{W}_\parallel &= 0 & \tilde{y}^T {}^\perp \tilde{W}_\perp &= 0 \end{aligned}$$

as \tilde{x}, \tilde{y} have only one non-zero term, which does not correspond to a non-zero term in the components of \tilde{W} in the equations.

Then, defining ${}^\parallel W_\parallel = U^T {}^\parallel \tilde{W}_\parallel V$, and the other components analogously, we get equations of the form

$${}^\parallel W_\perp x = U^T {}^\parallel \tilde{W}_\perp Vx = U^T {}^\parallel \tilde{W}_\perp \tilde{x} = 0$$

□

Observation 3. Given W, x as before, and considering W_\parallel, W_\perp with respect to x (wlog a unit vector) we can express them directly in terms of W as follows: Letting $W^{(i)}$ be the i th row of W , we have

$$W_{\parallel} = \begin{pmatrix} ((W^{(0)})^T \cdot x)x \\ \vdots \\ ((W^{(k)})^T \cdot x)x \end{pmatrix}$$

i.e. the projection of each row in the direction of x . And of course

$$W_{\perp} = W - W_{\parallel}$$

The motivation to consider such a decomposition of W is for the resulting independence between different components, as shown in the following lemma.

Lemma 2. Independence of Projections *Let x be a given vector (wlog of unit norm.) If W is a random matrix with $W_{ij} \sim \mathcal{N}(0, \sigma^2)$, then W_{\parallel} and W_{\perp} with respect to x are independent random variables.*

Proof. There are two possible proof methods:

- (a) We use the rotational invariance of random Gaussian matrices, i.e. if W is a Gaussian matrix, iid entries $\mathcal{N}(0, \sigma^2)$, and R is a rotation, then RW is also iid Gaussian, entries $\mathcal{N}(0, \sigma^2)$. (This follows easily from affine transformation rules for multivariate Gaussians.)

Let V be a rotation as in Lemma 1. Then $\tilde{W} = WV^T$ is also iid Gaussian, and furthermore, \tilde{W}_{\parallel} and \tilde{W}_{\perp} partition the entries of \tilde{W} , so are evidently independent. But then $W_{\parallel} = \tilde{W}_{\parallel}V^T$ and $W_{\perp} = \tilde{W}_{\perp}V^T$ are also independent.

- (b) From the observation note that W_{\parallel} and W_{\perp} have a centered multivariate joint Gaussian distribution (both consist of linear combinations of the entries W_{ij} in W .) So it suffices to show that W_{\parallel} and W_{\perp} have covariance 0. Because both are centered Gaussians, this is equivalent to showing $\mathbb{E}(\langle W_{\parallel}, W_{\perp} \rangle) = 0$. We have that

$$\mathbb{E}(\langle W_{\parallel}, W_{\perp} \rangle) = \mathbb{E}(W_{\parallel}W_{\perp}^T) = \mathbb{E}(W_{\parallel}W^T) - \mathbb{E}(W_{\parallel}W_{\parallel}^T)$$

As any two rows of W are independent, we see from the observation that $\mathbb{E}(W_{\parallel}W^T)$ is a diagonal matrix, with the i th diagonal entry just $((W^{(0)})^T \cdot x)^2$. But similarly, $\mathbb{E}(W_{\parallel}W_{\parallel}^T)$ is also a diagonal matrix, with the same diagonal entries - so the claim follows. □

In the following two lemmas, we use the rotational invariance of Gaussians as well as the chi distribution to prove results about the expected norm of a random Gaussian vector.

Lemma 3. Norm of a Gaussian vector *Let $X \in \mathbb{R}^k$ be a random Gaussian vector, with X_i iid, $\sim \mathcal{N}(0, \sigma^2)$. Then*

$$\mathbb{E}[\|X\|] = \sigma\sqrt{2} \frac{\Gamma((k+1)/2)}{\Gamma(k/2)}$$

Proof. We use the fact that if Y is a random Gaussian, and $Y_i \sim \mathcal{N}(0, 1)$ then $\|Y\|$ follows a chi distribution. This means that $\mathbb{E}(\|X\|/\sigma) = \sqrt{2}\Gamma((k+1)/2)/\Gamma(k/2)$, the mean of a chi distribution with k degrees of freedom, and the result follows by noting that the expectation in the lemma is σ multiplied by the above expectation. □

We will find it useful to bound ratios of the Gamma function (as appear in Lemma 3) and so introduce the following inequality, from [35] that provides an extension of Gautschi's Inequality.

Theorem 6. An Extension of Gautschi's Inequality *For $0 < s < 1$, we have*

$$\left(x + \frac{s}{2}\right)^{1-s} \leq \frac{\Gamma(x+1)}{\Gamma(x+s)} \leq \left(x - \frac{1}{2} + \left(s + \frac{1}{4}\right)^{\frac{1}{2}}\right)^{1-s}$$

We now show:

Lemma 4. Norm of Projections *Let W be a k by k random Gaussian matrix with iid entries $\sim \mathcal{N}(0, \sigma^2)$, and x, y two given vectors. Partition W into components as in Lemma 1 and let x_\perp be a nonzero vector perpendicular to x . Then*

(a)

$$\mathbb{E} [\|^\perp W_\perp x_\perp\|] = \|x_\perp\| \sigma \sqrt{2} \frac{\Gamma(k/2)}{\Gamma((k-1)/2)} \geq \|x_\perp\| \sigma \sqrt{2} \left(\frac{k}{2} - \frac{3}{4} \right)^{1/2}$$

(b) *If $\mathbb{1}_\mathcal{A}$ is an identity matrix with non-zeros diagonal entry i iff $i \in \mathcal{A} \subset [k]$, and $|\mathcal{A}| > 2$, then*

$$\mathbb{E} [\|\mathbb{1}_\mathcal{A}^\perp W_\perp x_\perp\|] \geq \|x_\perp\| \sigma \sqrt{2} \frac{\Gamma(|\mathcal{A}|/2)}{\Gamma((|\mathcal{A}|-1)/2)} \geq \|x_\perp\| \sigma \sqrt{2} \left(\frac{|\mathcal{A}|}{2} - \frac{3}{4} \right)^{1/2}$$

Proof. (a) Let U, V, \tilde{W} be as in Lemma 1. As U, V are rotations, \tilde{W} is also iid Gaussian. Furthermore for any fixed W , with $\tilde{a} = Va$, by taking inner products, and square-rooting, we see that $\|\tilde{W}\tilde{a}\| = \|Wa\|$. So in particular

$$\mathbb{E} [\|^\perp W_\perp x_\perp\|] = \mathbb{E} [\|^\perp \tilde{W}_\perp \tilde{x}_\perp\|]$$

But from the definition of non-zero entries of $^\perp \tilde{W}_\perp$, and the form of \tilde{x}_\perp (a zero entry in the first coordinate), it follows that $^\perp \tilde{W}_\perp \tilde{x}_\perp$ has exactly $k-1$ non zero entries, each a centered Gaussian with variance $(k-1)\sigma^2 \|x_\perp\|^2$. By Lemma 3, the expected norm is as in the statement. We then apply Theorem 6 to get the lower bound.

(b) First note we can view $\mathbb{1}_\mathcal{A}^\perp W_\perp = ^\perp \mathbb{1}_\mathcal{A} W_\perp$. (Projecting down to a random (as W is random) subspace of fixed size $|\mathcal{A}| = m$ and then making perpendicular commutes with making perpendicular and then projecting everything down to the subspace.)

So we can view W as a random m by k matrix, and for x, y as in Lemma 1 (with y projected down onto m dimensions), we can again define U, V as k by k and m by m rotation matrices respectively, and $\tilde{W} = UWV^T$, with analogous properties to Lemma 1. Now we can finish as in part (a), except that $^\perp \tilde{W}_\perp \tilde{x}$ may have only $m-1$ entries, (depending on whether y is annihilated by projecting down by $\mathbb{1}_\mathcal{A}$) each of variance $(k-1)\sigma^2 \|x_\perp\|^2$.

□

Lemma 5. Norm and Translation *Let X be a centered multivariate Gaussian, with diagonal covariance matrix, and μ a constant vector.*

$$\mathbb{E}(\|X - \mu\|) \geq \mathbb{E}(\|X\|)$$

Proof. The inequality can be seen intuitively geometrically: as X has diagonal covariance matrix, the contours of the pdf of $\|X\|$ are circular centered at 0, decreasing radially. However, the contours of the pdf of $\|X - \mu\|$ are shifted to be centered around $\|\mu\|$, and so shifting back μ to 0 reduces the norm.

A more formal proof can be seen as follows: let the pdf of X be $f_X(\cdot)$. Then we wish to show

$$\int_x \|x - \mu\| f_X(x) dx \geq \int_x \|x\| f_X(x) dx$$

Now we can pair points $x, -x$, using the fact that $f_X(x) = f_X(-x)$ and the triangle inequality on the integrand to get

$$\int_{|x|} (\|x - \mu\| + \|-x - \mu\|) f_X(x) dx \geq \int_{|x|} \|2x\| f_X(x) dx = \int_{|x|} (\|x\| + \|-x\|) f_X(x) dx$$

□

A.2 Proof of Theorem

Proof. We first prove the zero bias case, Theorem 1. To do so, it is sufficient to prove that

$$\mathbb{E} \left[\left\| \delta z^{(d+1)}(t) \right\| \right] \geq O \left(\left(\frac{\sqrt{\sigma k}}{\sqrt{\sigma} + k} \right)^{d+1} \right) \left\| \delta z^{(0)}(t) \right\| \quad (**)$$

as integrating over t gives us the statement of the theorem.

For ease of notation, we will suppress the t in $z^{(d)}(t)$.

We first write

$$W^{(d)} = W_{\perp}^{(d)} + W_{\parallel}^{(d)}$$

where the division is done with respect to $z^{(d)}$. Note that this means $h^{(d+1)} = W_{\parallel}^{(d)} z^{(d)}$ as the other component annihilates (maps to 0) $z^{(d)}$.

We can also define $\mathcal{A}_{W_{\parallel}^{(d)}} = \{i : i \in [k], |h_i^{(d+1)}| < 1\}$ i.e. the set of indices for which the hidden representation is not saturated. Letting W_i denote the i th row of matrix W , we now claim that:

$$\mathbb{E}_{W^{(d)}} \left[\left\| \delta z^{(d+1)} \right\| \right] = \mathbb{E}_{W_{\parallel}^{(d)}} \mathbb{E}_{W_{\perp}^{(d)}} \left[\left(\sum_{i \in \mathcal{A}_{W_{\parallel}^{(d)}}} ((W_{\perp}^{(d)})_i \delta z^{(d)} + (W_{\parallel}^{(d)})_i \delta z^{(d)})^2 \right)^{1/2} \right] \quad (*)$$

Indeed, by Lemma 2 we first split the expectation over $W^{(d)}$ into a tower of expectations over the two independent parts of W to get

$$\mathbb{E}_{W^{(d)}} \left[\left\| \delta z^{(d+1)} \right\| \right] = \mathbb{E}_{W_{\parallel}^{(d)}} \mathbb{E}_{W_{\perp}^{(d)}} \left[\left\| \phi(W^{(d)} \delta z^{(d)}) \right\| \right]$$

But conditioning on $W_{\parallel}^{(d)}$ in the inner expectation gives us $h^{(d+1)}$ and $\mathcal{A}_{W_{\parallel}^{(d)}}$, allowing us to replace the norm over $\phi(W^{(d)} \delta z^{(d)})$ with the sum in the term on the right hand side of the claim.

Till now, we have mostly focused on partitioning the matrix $W^{(d)}$. But we can also set $\delta z^{(d)} = \delta z_{\parallel}^{(d)} + \delta z_{\perp}^{(d)}$ where the perpendicular and parallel are with respect to $z^{(d)}$. In fact, to get the expression in (**), we derive a recurrence as below:

$$\mathbb{E}_{W^{(d)}} \left[\left\| \delta z_{\perp}^{(d+1)} \right\| \right] \geq O \left(\frac{\sqrt{\sigma k}}{\sqrt{\sigma} + k} \right) \mathbb{E}_{W^{(d)}} \left[\left\| \delta z_{\perp}^{(d)} \right\| \right]$$

To get this, we first need to define $\hat{z}^{(d+1)} = \mathbb{1}_{\mathcal{A}_{W_{\parallel}^{(d)}}} h^{(d+1)}$ - the latent vector $h^{(d+1)}$ with all saturated units zeroed out.

We then split the column space of $W^{(d)} = {}^{\perp}W^{(d)} + {}^{\parallel}W^{(d)}$, where the split is with respect to $\hat{z}^{(d+1)}$. Letting $\delta z_{\perp}^{(d+1)}$ be the part perpendicular to $z^{(d+1)}$, and \mathcal{A} the set of units that are unsaturated, we have an important relation:

Claim

$$\left\| \delta z_{\perp}^{(d+1)} \right\| \geq \left\| {}^{\perp}W^{(d)} \delta z^{(d)} \mathbb{1}_{\mathcal{A}} \right\|$$

(where the indicator in the right hand side zeros out coordinates not in the active set.)

To see this, first note, by definition,

$$\delta z_{\perp}^{(d+1)} = W^{(d)} \delta z^{(d)} \cdot \mathbb{1}_{\mathcal{A}} - \langle W^{(d)} \delta z^{(d)} \cdot \mathbb{1}_{\mathcal{A}}, \hat{z}^{(d+1)} \rangle \hat{z}^{(d+1)} \quad (1)$$

where the $\hat{\cdot}$ indicates a unit vector.

Similarly

$${}^\perp W^{(d)} \delta z^{(d)} = W^{(d)} \delta z^{(d)} - \langle W^{(d)} \delta z^{(d)}, \hat{z}^{(d+1)} \rangle \hat{z}^{(d+1)} \quad (2)$$

Now note that for any index $i \in \mathcal{A}$, the right hand sides of (1) and (2) are identical, and so the vectors on the left hand side agree for all $i \in \mathcal{A}$. In particular,

$$\delta z_{\perp}^{(d+1)} \cdot \mathbb{1}_{\mathcal{A}} = {}^\perp W^{(d)} \delta z^{(d)} \cdot \mathbb{1}_{\mathcal{A}}$$

Now the claim follows easily by noting that $\|\delta z_{\perp}^{(d+1)}\| \geq \|\delta z_{\perp}^{(d+1)} \cdot \mathbb{1}_{\mathcal{A}}\|$.

Returning to (*), we split $\delta z^{(d)} = \delta z_{\perp}^{(d)} + \delta z_{\parallel}^{(d)}$, $W_{\perp}^{(d)} = {}^\perp W_{\perp}^{(d)} + {}^\perp W_{\parallel}^{(d)}$ (and $W_{\parallel}^{(d)}$ analogously), and after some cancellation, we have

$$\mathbb{E}_{W^{(d)}} \left[\left\| \delta z^{(d+1)} \right\| \right] = \mathbb{E}_{W_{\parallel}^{(d)}} \mathbb{E}_{W_{\perp}^{(d)}} \left[\left(\sum_{i \in \mathcal{A}_{W_{\parallel}^{(d)}}} \left(({}^\perp W_{\perp}^{(d)} + {}^\perp W_{\parallel}^{(d)})_i \delta z_{\perp}^{(d)} + ({}^\perp W_{\parallel}^{(d)} + {}^\perp W_{\parallel}^{(d)})_i \delta z_{\parallel}^{(d)} \right)^2 \right)^{1/2} \right]$$

We would like a recurrence in terms of only perpendicular components however, so we first drop the $\|W_{\perp}^{(d)}\|, \|W_{\parallel}^{(d)}\|$ (which can be done without decreasing the norm as they are perpendicular to the remaining terms) and using the above claim, have

$$\mathbb{E}_{W^{(d)}} \left[\left\| \delta z_{\perp}^{(d+1)} \right\| \right] \geq \mathbb{E}_{W_{\parallel}^{(d)}} \mathbb{E}_{W_{\perp}^{(d)}} \left[\left(\sum_{i \in \mathcal{A}_{W_{\parallel}^{(d)}}} \left(({}^\perp W_{\perp}^{(d)})_i \delta z_{\perp}^{(d)} + ({}^\perp W_{\parallel}^{(d)})_i \delta z_{\parallel}^{(d)} \right)^2 \right)^{1/2} \right]$$

But in the inner expectation, the term ${}^\perp W_{\parallel}^{(d)} \delta z_{\parallel}^{(d)}$ is just a constant, as we are conditioning on $W_{\parallel}^{(d)}$. So using Lemma 5 we have

$$\mathbb{E}_{W_{\perp}^{(d)}} \left[\left(\sum_{i \in \mathcal{A}_{W_{\parallel}^{(d)}}} \left(({}^\perp W_{\perp}^{(d)})_i \delta z_{\perp}^{(d)} + ({}^\perp W_{\parallel}^{(d)})_i \delta z_{\parallel}^{(d)} \right)^2 \right)^{1/2} \right] \geq \mathbb{E}_{W_{\perp}^{(d)}} \left[\left(\sum_{i \in \mathcal{A}_{W_{\parallel}^{(d)}}} \left(({}^\perp W_{\perp}^{(d)})_i \delta z_{\perp}^{(d)} \right)^2 \right)^{1/2} \right]$$

We can then apply Lemma 4 to get

$$\mathbb{E}_{W_{\perp}^{(d)}} \left[\left(\sum_{i \in \mathcal{A}_{W_{\parallel}^{(d)}}} \left(({}^\perp W_{\perp}^{(d)})_i \delta z_{\perp}^{(d)} \right)^2 \right)^{1/2} \right] \geq \frac{\sigma}{\sqrt{k}} \sqrt{2} \frac{\sqrt{2|\mathcal{A}_{W_{\parallel}^{(d)}}| - 3}}{2} \mathbb{E} \left[\left\| \delta z_{\perp}^{(d)} \right\| \right]$$

The outer expectation on the right hand side only affects the term in the expectation through the size of the non-saturated set of units. Letting $p = \mathbb{P}(|h_i^{(d+1)}| < 1)$, and noting that we get a non-zero norm only if $|\mathcal{A}_{W_{\parallel}^{(d)}}| \geq 2$ (else we cannot project down a dimension), and for $|\mathcal{A}_{W_{\parallel}^{(d)}}| \geq 2$,

$$\sqrt{2} \frac{\sqrt{2|\mathcal{A}_{W_{\parallel}^{(d)}}| - 3}}{2} \geq \frac{1}{\sqrt{2}} \sqrt{|\mathcal{A}_{W_{\parallel}^{(d)}}|}$$

we get

$$\mathbb{E}_{W^{(d)}} \left[\left\| \delta z_{\perp}^{(d+1)} \right\| \right] \geq \frac{1}{\sqrt{2}} \left(\sum_{j=2}^k \binom{k}{j} p^j (1-p)^{k-j} \frac{\sigma}{\sqrt{k}} \sqrt{j} \right) \mathbb{E} \left[\left\| \delta z_{\perp}^{(d)} \right\| \right]$$

We use the fact that we have the probability mass function for an (k, p) binomial random variable to bound the \sqrt{j} term:

$$\begin{aligned} \sum_{j=2}^k \binom{k}{j} p^j (1-p)^{k-j} \frac{\sigma}{\sqrt{k}} \sqrt{j} &= -\binom{k}{1} p (1-p)^{k-1} \frac{\sigma}{\sqrt{k}} + \sum_{j=0}^k \binom{k}{j} p^j (1-p)^{k-j} \frac{\sigma}{\sqrt{k}} \sqrt{j} \\ &= -\sigma \sqrt{k} p (1-p)^{k-1} + k p \cdot \frac{\sigma}{\sqrt{k}} \sum_{j=1}^k \frac{1}{\sqrt{j}} \binom{k-1}{j-1} p^{j-1} (1-p)^{k-j} \end{aligned}$$

But by using Jensen's inequality with $1/\sqrt{x}$, we get

$$\sum_{j=1}^k \frac{1}{\sqrt{j}} \binom{k-1}{j-1} p^{j-1} (1-p)^{k-j} \geq \frac{1}{\sqrt{\sum_{j=1}^k j \binom{k-1}{j-1} p^{j-1} (1-p)^{k-j}}} = \frac{1}{\sqrt{(k-1)p+1}}$$

where the last equality follows by recognising the expectation of a binomial $(k-1, p)$ random variable. So putting together, we get

$$\mathbb{E}_{W^{(d)}} \left[\left\| \delta z_{\perp}^{(d+1)} \right\| \right] \geq \frac{1}{\sqrt{2}} \left(-\sigma \sqrt{k} p (1-p)^{k-1} + \sigma \cdot \frac{\sqrt{k} p}{\sqrt{1+(k-1)p}} \right) \mathbb{E} \left[\left\| \delta z_{\perp}^{(d)} \right\| \right] \quad (\text{a})$$

To lower bound p , we first note that as $h_i^{(d+1)}$ is a normal random variable with variance $\leq \sigma^2$, if $A \sim \mathcal{N}(0, \sigma^2)$

$$\mathbb{P}(|h_i^{(d+1)}| < 1) \geq \mathbb{P}(|A| < 1) \geq \frac{1}{\sigma \sqrt{2\pi}} \quad (\text{b})$$

where the last inequality holds for $\sigma \geq 1$ and follows by Taylor expanding $e^{-x^2/2}$ around 0. Similarly, we can also show that $p \leq \frac{1}{\sigma}$.

So this becomes

$$\begin{aligned} \mathbb{E} \left[\left\| \delta z^{(d+1)} \right\| \right] &\geq \left(\frac{1}{\sqrt{2}} \left(\frac{1}{(2\pi)^{1/4}} \frac{\sqrt{\sigma k}}{\sqrt{\sigma \sqrt{2\pi} + (k-1)}} - \sqrt{k} \left(1 - \frac{1}{\sigma} \right)^{k-1} \right) \right) \mathbb{E} \left[\left\| \delta z_{\perp}^{(d)} \right\| \right] \\ &= O \left(\frac{\sqrt{\sigma k}}{\sqrt{\sigma + k}} \right) \mathbb{E} \left[\left\| \delta z_{\perp}^{(d)} \right\| \right] \end{aligned}$$

Finally, we can compose this, to get

$$\mathbb{E} \left[\left\| \delta z^{(d+1)} \right\| \right] \geq \left(\frac{1}{\sqrt{2}} \left(\frac{1}{(2\pi)^{1/4}} \frac{\sqrt{\sigma k}}{\sqrt{\sigma \sqrt{2\pi} + (k-1)}} - \sqrt{k} \left(1 - \frac{1}{\sigma} \right)^{k-1} \right) \right)^{d+1} c \cdot \|\delta x(t)\|$$

with the constant c being the ratio of $\|\delta x(t)_{\perp}\|$ to $\|\delta x(t)\|$. So if our trajectory direction is almost orthogonal to $x(t)$ (which will be the case for e.g. random circular arcs, c can be seen to be ≈ 1 by splitting into components as in Lemma 1, and using Lemmas 3, 4.)

□

Result for non-zero bias In fact, we can easily extend the above result to the case of non-zero bias. The insight is to note that because $\delta z^{(d+1)}$ involves taking a *difference* between $z^{(d+1)}(t+dt)$ and $z^{(d+1)}(t)$, the bias term does not enter at all into the expression for $\delta z^{(d+1)}$. So the computations above hold, and equation (a) becomes

$$\mathbb{E}_{W^{(d)}} \left[\left\| \delta z_{\perp}^{(d+1)} \right\| \right] \geq \frac{1}{\sqrt{2}} \left(-\sigma_w \sqrt{k} p (1-p)^{k-1} + \sigma_w \cdot \frac{\sqrt{k} p}{\sqrt{1+(k-1)p}} \right) \mathbb{E} \left[\left\| \delta z_{\perp}^{(d)} \right\| \right]$$

We also now have that $h_i^{(d+1)}$ is a normal random variable with variance $\leq \sigma_w^2 + \sigma_b^2$ (as the bias is drawn from $\mathcal{N}(0, \sigma_b^2)$). So equation (b) becomes

$$\mathbb{P}(|h_i^{(d+1)}| < 1) \geq \frac{1}{\sqrt{(\sigma_w^2 + \sigma_b^2)}\sqrt{2\pi}}$$

This gives Theorem 1

$$\mathbb{E} \left[\left\| \delta z^{(d+1)} \right\| \right] \geq O \left(\frac{\sigma_w}{(\sigma_w^2 + \sigma_b^2)^{1/4}} \cdot \frac{\sqrt{k}}{\sqrt{\sqrt{\sigma_w^2 + \sigma_b^2} + k}} \right) \mathbb{E} \left[\left\| \delta z_{\perp}^{(d)} \right\| \right]$$

Statement and Proof of Upper Bound for Trajectory Growth Replace hard-tanh with a linear coordinate-wise identity map, $h_i^{(d+1)} = (W^{(d)} z^{(d)})_i + b_i$. This provides an upper bound on the norm. We also then recover a chi distribution with k terms, each with standard deviation $\frac{\sigma_w}{k^{\frac{1}{2}}}$,

$$\mathbb{E} \left[\left\| \delta z^{(d+1)} \right\| \right] \leq \sqrt{2} \frac{\Gamma((k+1)/2)}{\Gamma(k/2)} \frac{\sigma_w}{k^{\frac{1}{2}}} \left\| \delta z^{(d)} \right\| \quad (2)$$

$$\leq \sigma_w \left(\frac{k+1}{k} \right)^{\frac{1}{2}} \left\| \delta z^{(d)} \right\|, \quad (3)$$

where the second step follows from [36], and holds for $k > 1$.

B Proofs and additional results from Section 2.2.3

Proof of Theorem 2

Proof. For $\sigma_b = 0$:

For hidden layer $d < n$, consider neuron $v_1^{(d)}$. This has as input $\sum_{i=1}^k W_{i1}^{(d-1)} z_i^{(d-1)}$. As we are in the large σ case, we assume that $|z_i^{(d-1)}| = 1$. Furthermore, as signs for $z_i^{(d-1)}$ and $W_{i1}^{(d-1)}$ are both completely random, we can also assume wlog that $z_i^{(d-1)} = 1$. For a particular input, we can define $v_1^{(d)}$ as *sensitive* to $v_i^{(d-1)}$ if $v_i^{(d-1)}$ transitioning (to wlog -1) will induce a transition in node $v_1^{(d)}$. A sufficient condition for this to happen is if $|W_{i1}| \geq |\sum_{j \neq i} W_{j1}|$. But $X = W_{i1} \sim \mathcal{N}(0, \sigma^2/k)$ and $\sum_{j \neq i} W_{j1} = Y' \sim \mathcal{N}(0, (k-1)\sigma^2/k)$. So we want to compute $\mathbb{P}(|X| > |Y'|)$. For ease of computation, we instead look at $\mathbb{P}(|X| > |Y|)$, where $Y \sim \mathcal{N}(0, \sigma^2)$.

But this is the same as computing $\mathbb{P}(|X|/|Y| > 1) = \mathbb{P}(X/Y < -1) + \mathbb{P}(X/Y > 1)$. But the ratio of two centered independent normals with variances σ_1^2, σ_2^2 follows a Cauchy distribution, with parameter σ_1/σ_2 , which in this case is $1/\sqrt{k}$. Substituting this in to the cdf of the Cauchy distribution, we get that

$$\mathbb{P} \left(\frac{|X|}{|Y|} > 1 \right) = 1 - \frac{2}{\pi} \arctan(\sqrt{k})$$

Finally, using the identity $\arctan(x) + \arctan(1/x)$ and the Laurent series for $\arctan(1/x)$, we can evaluate the right hand side to be $O(1/\sqrt{k})$. In particular

$$\mathbb{P} \left(\frac{|X|}{|Y|} > 1 \right) \geq O \left(\frac{1}{\sqrt{k}} \right) \quad (c)$$

This means that in expectation, any neuron in layer d will be sensitive to the transitions of \sqrt{k} neurons in the layer below. Using this, and the fact the while $v_i^{(d-1)}$ might flip very quickly from say -1 to 1 , the gradation in the transition ensures that neurons in layer d sensitive to $v_i^{(d-1)}$ will transition at distinct times, we get the desired growth rate in expectation as follows: let $t^{(d)}$ be the number of transitions in layer d , and let $t_i^{(d)}$ be the number of transitions of neuron i in layer d . Let $T^{(d+1)}$ be a random variable for the number of transitions in layer $d+1$, and $T_i^{(d+1)}$ the

equivalent for neuron i . Then $\mathbb{E}[T^{(d+1)}] = \sum_i \mathbb{E}[T_i^{(d+1)}] = k\mathbb{E}[T_1^{(d+1)}]$ by symmetry. But $\mathbb{E}[T_1^{(d+1)}] \geq \mathbb{E}[\sum_i 1_{(1,i)} t_i^{(d+1)}]$ where $1_{(1,i)}$ is the indicator function of neuron 1 in layer $d+1$ being sensitive to neuron i in layer d . Using linearity of expectation and the result from above, we get $\mathbb{E}[T_1^{(d+1)}] \geq t^{(d)}/\sqrt{k}$. And so, using the fact that all transitions happen at distinct points almost surely, $\mathbb{E}[T^{(d+1)}] \geq \sqrt{k}t^{(d)}$.

For $\sigma_b > 0$:

We replace \sqrt{k} with $\sqrt{k(1 + \sigma_b^2/\sigma_w^2)}$, by noting that $Y \sim \mathcal{N}(0, \sigma_w^2 + \sigma_b^2)$. This results in a growth rate of form $O(\sqrt{k}/\sqrt{1 + \frac{\sigma_b^2}{\sigma_w^2}})$. \square

C Proofs and additional results from Section 2.3

Proof of Theorem 4

Proof. Let the hyperplane arrangement be denoted \mathcal{H} , and let $H \in \mathcal{H}$ be one specific hyperplane. Then the number of regions in \mathcal{H} is precisely the number of regions in $\mathcal{H} - H$ plus the number of regions in $\mathcal{H} \cap H$. (This follows from the fact that H subdivides into two regions exactly all of the regions in $\mathcal{H} \cap H$, and does not affect any of the other regions.)

In particular, we have the recursive formula

$$r(k, m) = r(k-1, m) + r(k-1, m-1)$$

We now induct on $k+m$ to assert the claim. The base cases of $r(1, 0) = r(0, 1) = 1$ are trivial, and assuming the claim for $\leq k+m-1$ as the induction hypothesis, we have

$$\begin{aligned} r(k-1, m) + r(k-1, m-1) &\leq \sum_{i=0}^m \binom{k-1}{i} + \sum_{i=0}^{m-1} \binom{k-1}{i} \\ &\leq \binom{k-1}{0} + \sum_{i=0}^{d-1} \binom{k-1}{i} + \binom{k-1}{i+1} \\ &\leq \binom{k}{0} + \sum_{i=0}^{m-1} \binom{k}{i+1} \end{aligned}$$

where the last equality follows by the well known identity

$$\binom{a}{b} + \binom{a}{b+1} = \binom{a+1}{b+1}$$

This concludes the proof. \square

D Proofs and additional results from Section 3

D.1 Upper Bound for Dichotomies

The Vapnik-Chervonenkis (VC) dimension of a function class is the cardinality of the largest set of points that it can shatter. The VC dimension provides an upper (worst case) bound on the generalization error for a function class [37]. Motivated by generalization error, VC dimension has been studied for neural networks [12, 13]. In [14] an upper bound on the VC dimension v of a neural network with piecewise polynomial activation function and binary output is derived. For hard-tanh units, this bound is

$$v = 2|W|n \log(4e|W|nk) + 2|W|n^2 \log 2 + 2n, \quad (4)$$

where $|W|$ is the total number of weights, n is the depth, and k is the width of the network. The VC dimension provides an upper bound on the number of achievable dichotomies $|\mathcal{F}|$ by way of the Sauer–Shelah lemma [33],

$$|\mathcal{F}| \leq \left(\frac{e|S|}{v} \right)^v. \quad (5)$$

By combining Equations 4 and 5 an upper bound on the number of dichotomies is found, with a growth rate which is exponential in a low order polynomial of the network size.